In search of a unifying theory of white matter aging: associations with age in perfusion detectable in advance of microstructure

Tyler D. Robinson[1], Yutong L. Sun[1], Paul T. H. Chang[1], J. Jean Chen[1,2,3]

1. Rotman Research Institute, Baycrest, Canada
2. Medical Biophysics, University of Toronto, Canada
3. Biomedical Engineering, University of Toronto, Canada

ABSTRACT

One of the most promising interventional targets for brain health is cerebral perfusion, but its link to white matter (WM) aging remains unclear. Motivated by existing literature demonstrating links between declining cortical perfusion and the development of WM hyperintensities, we posit that regional WM hypoperfusion precedes deteriorating WM integrity. Using the Human Connectome Project Aging (HCP-A) data set, we examine tract-wise associations between WM microstructural integrity (i.e. fractional anisotropy, mean diffusivity, axial diffusivity, and radial diffusivity) and perfusion (i.e. cerebral blood flow and arterial transit time) in ten major bilateral WM tracts. Results show that WM perfusion-microstructure relationships vary by both tract and sex. Moreover, we identify multiple distinct stages of deterioration, with female subjects demonstrating more tracts in advanced stages of decline. Additionally, arterial transit time appears to be the earliest indicator of WM declines, preceding age-related microstructural differences in several tracts. This study contributes compelling evidence to the vascular hypothesis of WM degeneration, and highlights the utility of blood-flow timing as an early marker of aging.

Keywords: White Matter, Aging, Diffusion, Perfusion, Microstructure, Tractography

INTRODUCTION

Increasing appreciation for the importance of cerebrovascular health in maintaining tissue integrity has led to the examination of tissue structure-perfusion associations in brain aging. The existing literature has focused largely on gray matter (GM) perfusion and its associations with cortical and subcortical atrophy (Baker et al., 2014; Chen et al., 2011, 2013; C.-M. Kim et al., 2020; Mayer et al., 2021). In the white matter (WM), microstructural declines in aging are reported in a robust body of literature, demonstrating regional differences in age-related microstructural declines along both broad regional and tract-specific segmentations (Baker et al., 2014; Bender et al., 2016; de Groot et al., 2015, 2016; Sala et al., 2012; Slater et al., 2019). Furthermore, recent investigation of tract-wise differences in patterns of microstructural and morphometric decline (Schilling et al., 2022), as well as in relationships between WM integrity and tract morphometry (Robinson et al., 2023), suggest that microstructural variations in different tracts are differentially associated with morphometric declines with age. However, the basis of this heterogeneity between tracts remains unclear. These findings cumulatively suggest that a more complete understanding of the interrelations between perfusion and integrity in the WM on a tract-specific basis is necessary to clarify patterns of decline across the brain.

A well-established relationship between cortical perfusion and the development of WM hyperintensities in associated subcortical regions illustrates the importance of CBF to maintaining the integrity of WM fibers (Bernbaum et al., 2015; O'Sullivan et al., 2002). Cortical perfusion was further related to subcortical WM integrity in normal aging (Chen et al., 2013). Relationships have been demonstrated between cortical perfusion and cognitive performance (D. Kim et al., 2021), and decreased cortical perfusion may predict heightened vulnerability to pathological declines (Chen et al., 2013; Mayer et al., 2021; O'Sullivan et al., 2002). However, regional variation in age-related cortical atrophy does not appear to match regional reductions in cerebral blood flow (CBF) (Chen et al., 2011), suggesting a potential temporal asynchrony in perfusion and structural effects of age. Such an asynchrony, with perfusion decline preceding structural decline, would be consistent with the vascular hypothesis of aging and dementia (de la Torre, 2018), but has yet to be confirmed despite promising evidence that CBF

changes precede structural degeneration changes in the GM (Lee, 2022; Wierenga et al., 2014; Zlokovic, 2011). Moreover, investigations of this nature are much scarcer in the WM, despite the latter manifesting age effects earlier than GM (Giorgio et al., 2010).

With changes in cortical perfusion leading declines in the WM, regional perfusion in the WM itself presents a strong candidate as an early imaging marker of age-related declines in WM microstructure should WM perfusion declines similarly lead microstructural degeneration. However, the structural-perfusion relationship in the aging WM has not been examined, largely due to challenges in WM perfusion quantification (Bernbaum et al., 2015; Chen et al., 2013). By incorporating regional perfusion measures into our ongoing model of WM microstructural and morphometric declines with age (Robinson et al., 2023), we aim to build a more comprehensive understanding of the mechanisms of WM decline and improve early detection of pathological WM changes.

To some extent, patterns of WM decline and resilience appear to broadly follow developmental trajectories, though support for ordered models is mixed (Hoagey et al., 2019; Slater et al., 2019; Stricker et al., 2009). With regards to vascular development, vessels in frontal and cerebrospinal tracts develop in the embryo prior to those in the parietal and posterior brain, supporting the development of their respective WM regions (Smirnov et al., 2021). This raises differences in vascularization as a potential source of later differences in rates and patterns of WM declines. These lines of evidence encourage a tract-wise determination of perfusion-microstructural associations, whereby those tracts or regions that demonstrate greater robustness to age-related declines are differentiated from more susceptible regions by differences in underlying vascular decline, potentially related to the manner in which blood vessels developed. However, due to the limited robustness of WM regional perfusion quantification, there is limited understanding of regional variation in WM perfusion metrics and how they relate to microstructural declines locally. Unlike the cortical surface, which is fed by larger penetrating vessels, blood supply to the WM is fed primarily by smaller vessels entering from either the cortical surface or the midbrain (Nonaka et al., 2003; Smirnov et al., 2021). This results in both (1) considerable variation in proximity to major vessels and number of blood flow sources and (2) the likelihood that vascular disease

and age-related deterioration that differentially affects small vessels has an earlier impact on the WM than on the cortical surface (Akashi et al., 2017; Hase et al., 2018). Tractwise heterogeneity in blood vessel development may then underlie susceptibility to age-related changes in perfusion and regional ability to support continued microstructural integrity with age.

Vascular declines with age have been consistently demonstrated in the WM as part of general systemic vascular decline (Kohn et al., 2015; Li et al., 2018; Tomoto et al., 2023). Increasing arterial stiffness due to the progressive decay of elastin in normal aging results in more fragile blood vessels (Kohn et al., 2015; Tomoto et al., 2023). Even in intact arterial pathways, changes in vessel morphometry result in more tortuous micro- and meso-vasculature with reduced blood flow (Li et al., 2018). As a result, diminished perfusion into WM tissues is expected in healthy aging. As prior research has demonstrated an association between reduced perfusion in the cortex and the development of WM hyperintensities in related WM regions (Mayer et al., 2021), it is intuitive that changes in perfusion in the WM precede declines in WM integrity and ultimately the breakdown of WM tissue. This process likely results from the progressive inability of supporting glial cells to maintain myelin in WM fibers as perfusion (CBF) declines (Kobayashi et al., 2002; Kohama et al., 2012). Those axons with reduced or malformed myelin sheaths are then more vulnerable to age-related culling of vulnerable WM fibers, and associated WM regions at higher risk of pathological declines (Kohama et al., 2012; Tang et al., 1997). Related to cerebrovascular mapping, vascular response latency has been demonstrated as a more sensitive marker of pathology than response amplitude (Holmes et al., 2020; D. Kim et al., 2021; McKetton et al., 2019; Nanayakkara et al., 2023). Additionally, arterial-transit time (ATT) has been found to increase with advancing age (Mutsaerts et al., 2015). Moreover, arterial-transit time has been found to be independently related to white-matter lesions relative to CBF (Zhang et al., 2018). Thus, it is also interesting to determine whether CBF or ATT is an earlier marker of possible WM degeneration.

Given the previously limited ability to measure regional differences in WM perfusion (Bernbaum et al., 2015; Chen et al., 2013) and a relative sparsity of studies addressing WM vascular-microstructural declines on a tractwise basis (Mayer et al., 2021; Smirnov et al., 2021), this study aims to fill both of

these knowledge gaps, with the understanding that WM tracts represent the meaningful structural units for segmentation of the WM (Baker et al., 2014; Sala et al., 2012; Yeatman et al., 2014) in aging, as well as reflecting functional connections between terminal cortical regions (Nozais et al., 2021). As variability in tractwise perfusion remains underexplored in healthy adults, it represents a natural extension to existing literature and a valuable missing component in modeling regional WM declines with age and may represent an underlying source of differences in order and rate of tractwise declines. Using the Human Connectome Project Aging (HCP-A) data set (Bookheimer et al., 2019), this study sought to map tractwise age-related variations in WM perfusion, as well as the relationships between tractwise WM perfusion and microstructure. We hypothesized that (1) tract perfusion and microstructure will not decline at the same rate at aging, that is to say that (2) tractwise perfusion changes will be detectable at younger ages than microstructural declines.

METHODS

This study includes five hundred and thirty-five healthy adult subjects (300 female, aged 36-100) from the Human Connectome Project in Aging (HCP-A) dataset (OMB Control# 0925-0667 (Bookheimer et al., 2019; Harms et al., 2018). All subjects were in generally good health and without pathological cognitive impairment (i.e. stroke, clinical dementia). Following manual quality control, thirty-two subjects were excluded from this sample due to MRI artifacts that produced notable errors when generating WM masks. Three additional subjects were excluded as age outliers due to being the only subjects of 100 years of age. Thus, the final sample size was 500 subjects (249 female, aged 36-89).

The study accessed whole-brain T1-weighted structural MRI, diffusion-weighted MRI (dMRI) with a $(1.5mm)^3$ voxel resolution, MB=4, with 93 directions at $b=1500s/mm^2$, and multi-delay multi-band echo planar imaging (MB-EPI) pseudo-continuous arterial spin labeling (pCASL) with a $(2.5mm)^3$ voxel resolution, MB=6, with TIs = 0.7, 1.2, 1.7, 2.2, and 2.7, collected using four matched Siemens Prisma 3T MRI scanners. Further imaging parameters for structural, diffusion, and perfusion imaging can be found in (Harms et al., 2018).

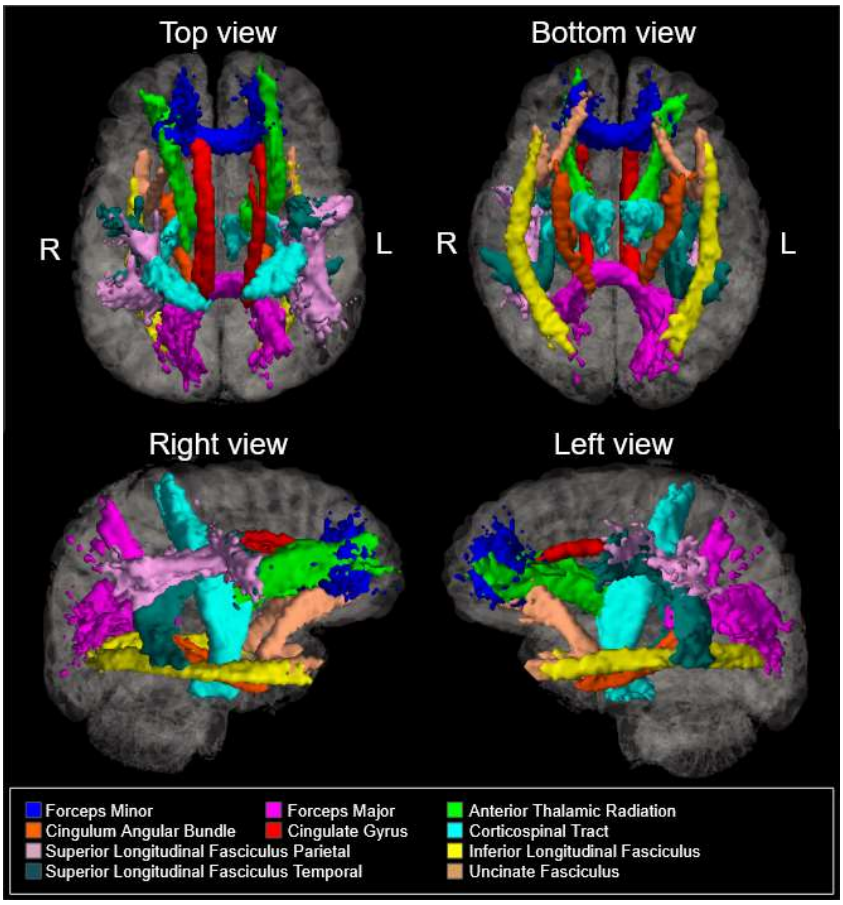

Figure 1: Ten bilateral tracts of interest reconstructed Freesurfer's TRACULA package. Note that there is limited overlap between tracts.

Image analysis

dMRI data were corrected for eddy-current and susceptibility-related distortions via EDDY prior to use in tractography analysis. Eighteen major WM tracts were reconstructed from the dMRI data using the Tracts Constrained by Underlying Anatomy (TRACULA) tool in Freesurfer version 7.2.0 (Maffei et al., 2021; Yendiki et al., 2011). FSL's fslmaths function was then used to produce per-subject masks of each WM tract in local space. The eighteen reconstructed tracts were combined bilaterally to produce ten tracts of interest for analysis: The major forceps (Fmajor), minor forceps (Fminor), anterior thalamic radiation (ATR), cingulum angular bundle (CAB), cingulate gyrus (CCG), corticospinal tract (CST), inferior longitudinal fasciculus (ILF), superior longitudinal fasciculus parietal (SLFP), superior longitudinal fasciculus temporal (SLFT), and the uncinate fasciculus (UNC). (**Figure 1**). Rosner's tests were performed to identify and exclude volume outliers per tract in single tract analyses. The resulting subject counts for these analyses were: Fmajor (N=493), Fminor (N=493), ATR (N=497), CAB (N=490), CCG (N=495), CST (N=491), ILF (N=497), SLFP (N=497), SLFT (N=495), and UNC (N=495).

Microstructure

WM microstructural integrity was quantified using fractional anisotropy (FA), mean diffusivity (MD), axial diffusivity (AD), and radial diffusivity (AD). FA, MD, AD, and RD maps were derived via Dipy's DKI script to achieve kurtosis-corrected DTI metric fitting, due to the high b-value used in the HCP-A acquisitions. TRACULA generated tract masks were applied to local dMRI images in flsmaths to generate tract means for FA, MD, AD, and RD. For each metric, baseline normalized (percent of baseline) values ("FA_{perc}", "MD_{perc}", "AD_{perc}", "RD_{perc}") were calculated as individual raw tract values divided by the mean raw tract value of the youngest 10% of subjects to assess percent differences from the youngest baseline.

Perfusion

Perfusion metrics of interest to this study included cerebral blood flow (CBF) and arterial transit time (ATT). CBF was quantified using the general kinetic model that accounts for arterial-transit delay (FSL oxford_ASL) to produce local CBF and ATT maps. As with microstructure, TRACULA-generated tract masks were applied to the local maps in fslmaths to produce tract means for both perfusion metrics. Baseline normalized perfusion values ("CBF_{perc}", "ATT_{perc}") were again calculated as individual raw tract values divided by the mean raw tract value of the youngest 10% of subjects (i.e. the baseline group).

Statistical analysis

Age and sex effects

Between-subjects ANOVA was used to determine the presence of sex differences in tract specific FA_{perc}, MD_{perc}, CBF_{perc}, and ATT_{perc}. Subsequent assessment of sex differences in microstructure and perfusion were conducted for each tract via sequential multivariate regressions of sex on to mean FA_{perc}, MD_{perc}, CBF_{perc}, and ATT_{perc} using age as a covariate of no interest. Whole-WM age-related microstructure and perfusion differences were assessed via multivariate quadratic regression by first regressing age onto mean FA_{perc}, MD_{perc},CBF_{perc}, and ATT_{perc} values derived from voxel-count weighted

tract averages using sex as a covariate of no interest. This process was repeated for each tract separately in tract-wise analyses. FDR adjustment was again applied to the resulting p-values.

Microstructure vs Perfusion

Two multivariate regression models were constructed to assess relationships between microstructure, perfusion, age, and sex in our sample. Both models were applied first to whole-WM MD_{perc} and FA_{perc} values, then to each tract:

- *Model 1. microstructure vs. perfusion across ages:* assesses the degree to which perfusion metrics account for the age-related variability in mean normalized tract MD and FA, with subject sex as a covariate of no interest. That is,
    - $\{FA_{perc}, MD_{perc}\} = f(CBF_{perc}+Sex)$
    - $\{FA_{perc}, MD_{perc}\} = f(ATT_{perc}+Sex)$
- *Model 2. microstructure vs. perfusion between sexes:* assess the degree to which perfusion metrics account for sex-related differences in normalized tract MD and FA, with subject age as a covariate of no interest. That is,
    - $\{FA_{perc}, MD_{perc}\} = f(CBF_{perc}+Age)$
    - $\{FA_{perc}, MD_{perc}\} = f(ATT_{perc}+Age)$
    - One set of models is produced for each sex.

The above analyses were conducted in R (version 4.1.1).

Multimodal associations: Canonical correlation analysis (CCA)

Canonical correlation analysis (CCA) was conducted to examine the degrees to which each of our variables of interest contributed to age-related associations between microstructure and perfusion, respectively. Two column vectors were computed using our perfusion (V_1) variables (CBF_{perc}, ATT_{perc}) and microstructural (U_1) variables (AD_{perc}, RD_{perc}, FA_{perc}) in Matlab. The linear combinations of V and U vectors which produced the highest correlation were then calculated to determine on a tractwise basis

which variables loaded most strongly to correlated (between perfusion and microstructure) age differences by tract. This and following analyses substituted AD and RD variables for the MD variable used in previous analyses as examining the two orthogonal axes of diffusion separately was more meaningful for clarifying relationships between FA and other diffusion metrics as they relate to microstructural deterioration.

Time-lag analysis: cross-correlation function (CCF)

Cross-correlations functions (CCF) were calculated in Matlab (Mathworks, Natick, USA) to determine the presence of age-lagged relationships between each measure for perfusion and microstructure. Only variables demonstrating significant non-linear age effects on a tractwise basis were examined in this analysis to reduce ambiguity in CCF interpretation. A curvature threshold for age effects of 0.0005 was implemented, where curvature was computed using Matlab's *curvature* function. CCFs were calculated based on the models of age effects for six paired tractwise microstructure/morphometry measures, along with cross-comparisons for AD_{perc}/RD_{perc} vs FA_{perc} and CBF_{perc} vs ATT_{perc}:

- CBF vs. Microstructure: CBF_{perc} vs AD_{perc}, CBF_{perc} vs RD_{perc}, CBF_{perc} vs FA_{perc}
- ATT vs. Microstructure: ATT_{perc} vs AD_{perc}, ATT_{perc} vs RD_{perc}, ATT_{perc} vs FA_{perc}
- AD_{perc} vs FA_{perc}
- RD_{perc} vs FA_{perc}
- CBF_{perc} vs ATT_{perc}

3 RESULTS

Age differences

Significant linear and quadratic relationships between age and CBF_{perc} were identified in all tracts but UNC, with quadratic regressions providing a better fit as indicated by higher $R^2_{adjusted}$ in all tracts with the exception of Fminor and CCG. Significant associations were also identified between age and ATT_{perc} in Fmajor, ILF, and UNC, along with significant linear effects in Fminor, ATR, CCG, CST, SLFP, SLFT,

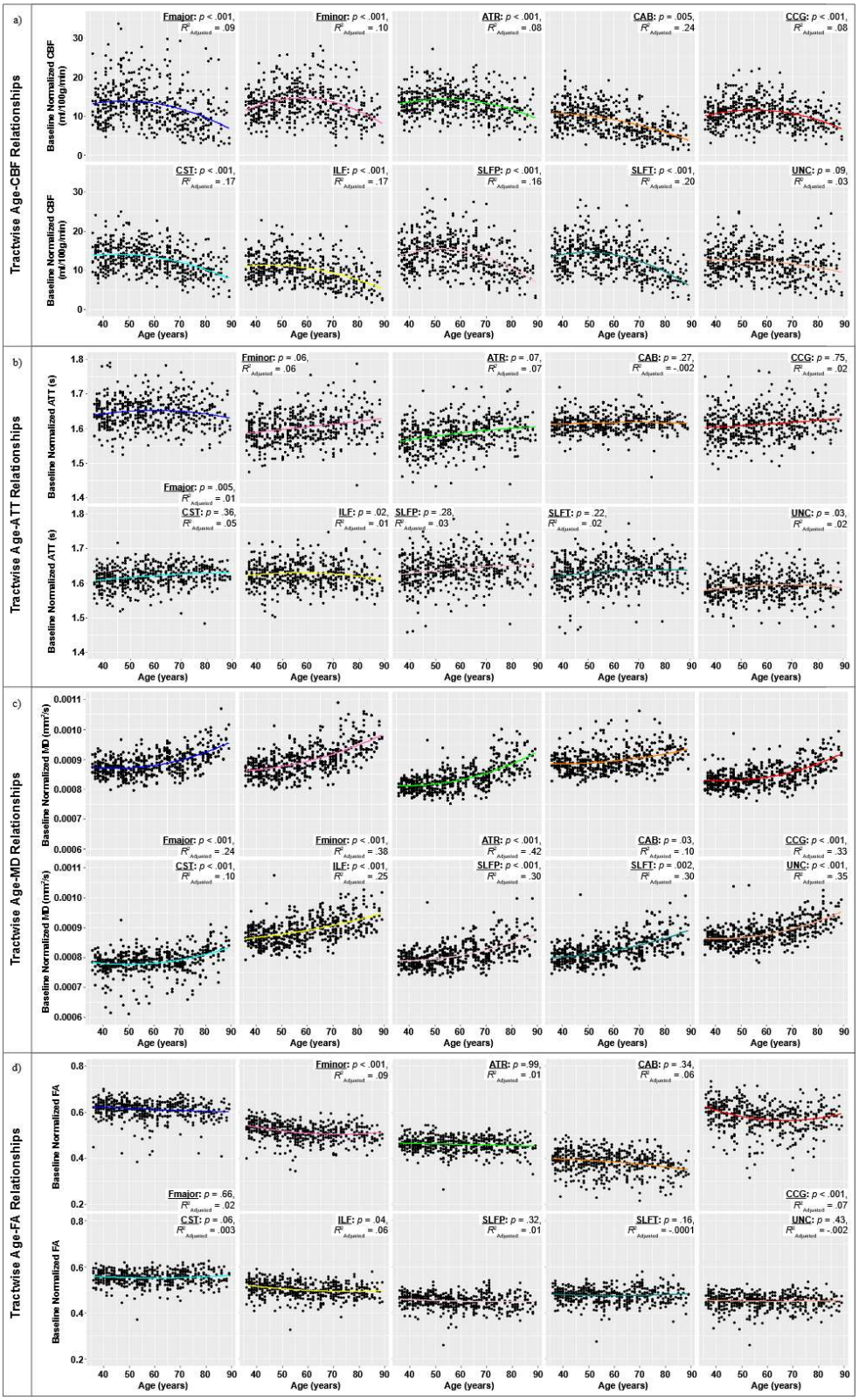

Figure 2: Tractwise quadratic regression of age effects on baseline normalized CBF, ATT, MD, and FA, with each dot representing one subject. The p-values and effect sizes (R2adjusted) from the quadratic fit are noted for each tract.

and UNC, with quadratic regression providing a better fit in UNC. Significant linear and quadratic relationships between age and MD_{perc} were identified in all tracts of interest, with quadratic regressions providing a better fit in all tracts. Lastly, significant quadratic associations between age and FA_{perc} were found in Fminor, CCG, and ILF, with significant linear associations in Fmajor, Fminor, ATR, CAB, CCG, ILF, SLFP.

Quadratic regression

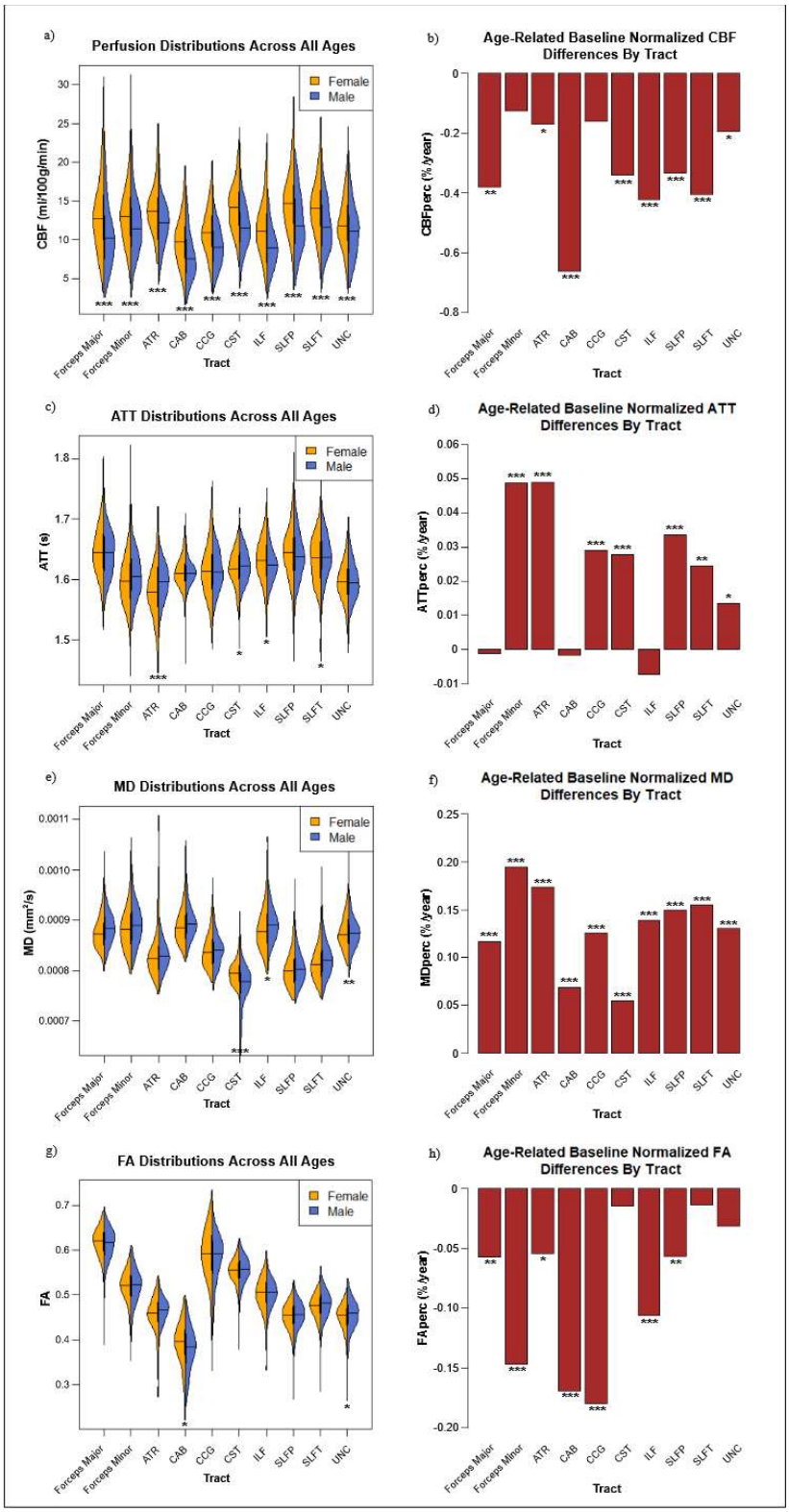

*Figure 3: Raw distributions separated by sex (a,d,g,j), whole-WM age effects (b,e,h,k), and tractwise age effects (c,f,j,l) for CBF, ATT, MD, and FA respectively. Significant effects by sex and age are denoted with asterisks (***: p<.001, **: p<.01, and *: p<.05).*

provided a better fit for the effects of age on FA in Fminor and CCG (**Figure 2**).

Sex differences

Female subjects showed significantly higher MD_{perc} in the Fmajor, ATR, CST, ILF, SLFP, and SLFT in regression analysis. While female subjects also demonstrated higher FA_{perc} in the Fmajor, male subjects showed higher FA_{perc} in the Fminor, CCG, SLFP, and SLFT. Female subjects demonstrated higher CBF_{perc} in the CAB, while male subjects showed higher CBF_{perc} in the ATR. Female subjects showed higher ATT_{perc} in the SLFP and SLFT, while male subjects showed higher ATT_{perc} in the ILF. (**Figure 3**)

Microstructure-perfusion relationships

Regression analyses

Model 1 (perfusion vs microstructure): Significant relationships were identified between CBF_{perc} and MD_{perc} ($F(2, 497) = 5.36$, $p = .005$, $R^2_{Adjusted} = .02$, slope = -0.02), as well as between ATT_{perc} and MD_{perc} ($F(2, 497) = 4.07$, $p = .02$, $R^2_{Adjusted} = .01$, slope = 0.23). No significant whole-WM relationships were found between FA_{perc} and WM perfusion (**Supplementary Table 1a**).

Significant negative relationships were found between tractwise CBF_{perc} and MD_{perc} in the ILF and SLFT. Significant positive relationships between ATT_{perc} and MD_{perc} were identified in the Fminor, ATR, SLFP, and SLFT. A single significant positive association was found between CBF_{perc} and FA_{perc} in the CCG. A significant negative relationship between ATT_{perc} and FA_{perc} was identified in the ATR, along with a positive relationship in the CAB Tract-wise results are summarized in **Supplementary Table 1b**.

Model 2 (sex differences in perfusion-microstructure relationships): No significant relationships were identified between whole-WM microstructure and perfusion in Model 2 (**Supplementary Table 2a**). After dividing the sample by sex, significant positive associations were found between CBF_{perc} and FA_{perc} in the CCG in both female and male subjects, as well as in the ATR in female subjects alone. A single negative association between CBF_{perc} and FA_{perc} was found in the CST in male subjects. Female subjects also demonstrated both a negative association between ATT_{perc} and FA_{perc} in the ATR, and a positive association between ATT_{perc} and FA_{perc} in the CAB. No associations were identified between perfusion and MD after dividing the sample by sex. Tract-wise results are summarized in **Supplementary Table 2b.**

CCA results of multimodal associations

The CCA identified multiple patterns of association between microstructure and perfusion loadings in male and female subjects (**Figure 4**). Loadings are listed for significant canonical correlations using a threshold of 0.5. In female subjects, CBF_{perc} contributed significantly in eight tracts, while ATT_{perc} contributed significantly in seven. AD_{perc}, RD_{perc}, and FA_{perc} loaded significantly in five, six, and one tract respectively. In male subjects, CBF_{perc} loaded significantly in four tracts, while ATT_{perc} loaded

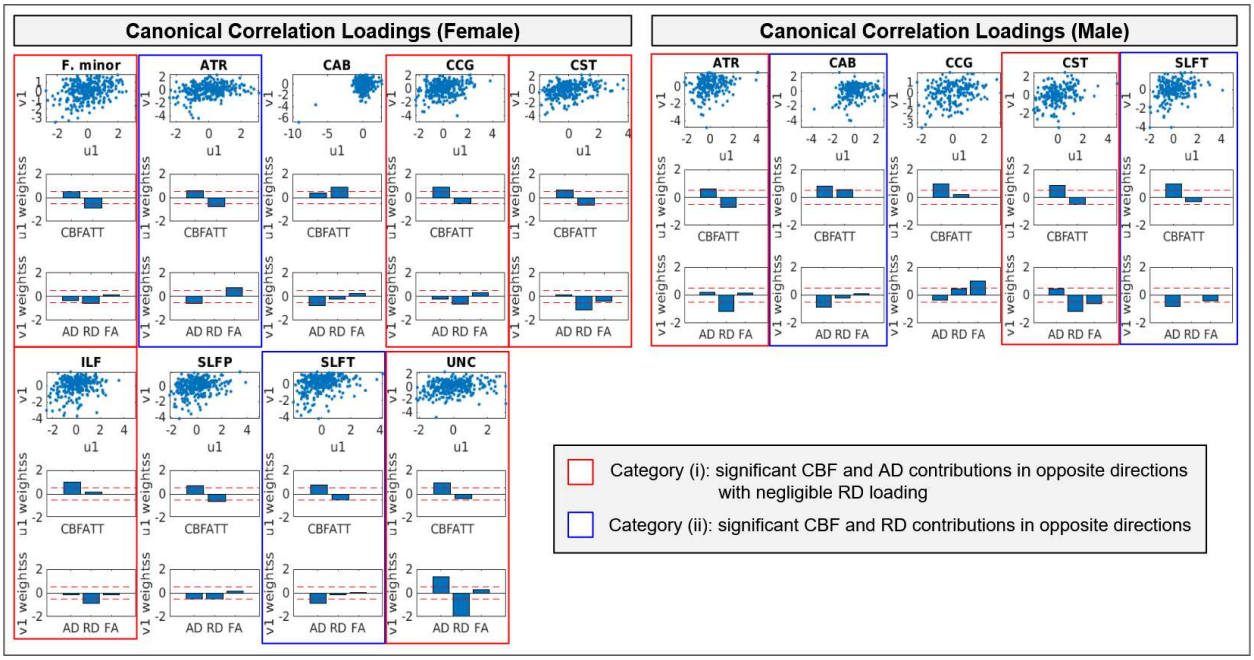

Figure 4: Tractwise contributions by perfusion (CBF/ATT) and microstructural (AD/RD/FA) measures to categorical perfusion-microstructure relationships separated by sex.

significantly in three. Male microstructural contributions showed significant loading by AD_{perc} in two tracts, RD_{perc} in two tracts, and FA_{perc} in two tracts.

Based on CCA results, tracts were further clustered in two loading signatures. Signature (i) was defined by tracts demonstrating significant CBF and AD contributions loading in opposite directions with negligible RD loading, suggesting early stages of degeneration, while signature (ii) was defined by opposing CBF and RD loading with matched or negligible AD contributions, suggesting more advanced degeneration. Two tracts exhibited signature (i) in female subjects (ATR, SLFT), along with five in pattern (ii) (Fminor, CCG, CST, ILF, UNC). In male subjects, Two tracts exhibited signature (i) (CAB, SLFT) with two tracts exhibiting signature (ii) (ATR, CST).

CCF results of time lags

At zero lag, significant correlations between CBF_{perc} and FA_{perc} were identified in Fmajor, CAB, CCG, CST, and SLFT, along with peak correlations at positive lag in the SLFP and UNC, such that FA_{perc} led CBF_{perc}. Significant zero-lag correlations were identified between CBF_{perc} and both AD_{perc} and RD_{perc}

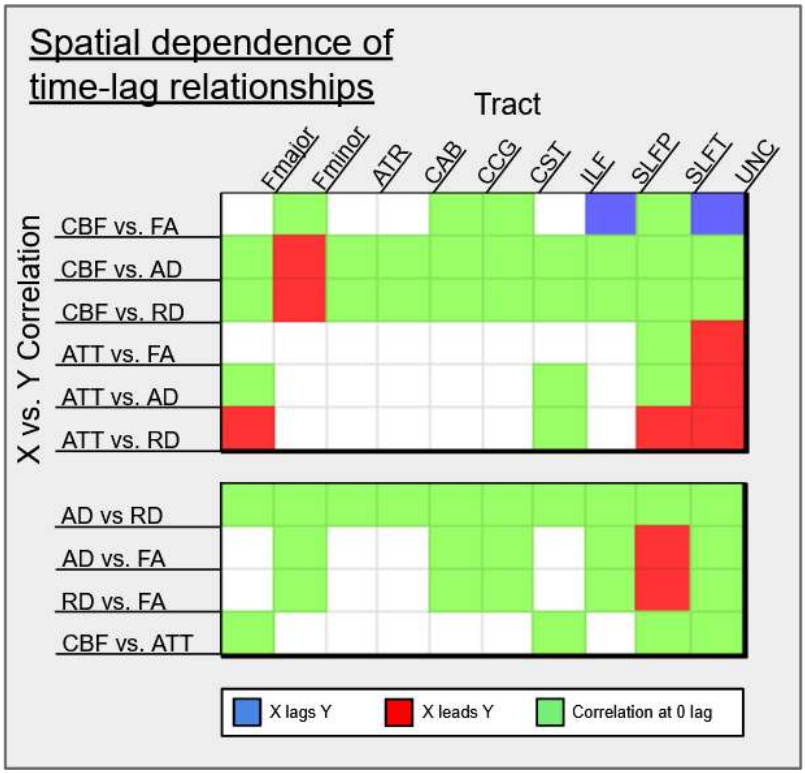

Figure 5: Tractwise cross-correlation results demonstrating significant peak correlations at positive, negative and zero lags.

in all tracts but the Fminor, in which peak correlations at negative lag were identified for both microstructural measures such that CBF_{perc} led AD_{perc}/RD_{perc}. A single significant zero-lag peak correlation was found between ATT_{perc} and FA_{perc} in the SLFT, along with a peak correlation at negative lag in the UNC. Significant zero-lag correlations were found between ATT_{perc} and AD_{perc} in the Fmajor, CST, and SLFP, along with a peak correlation at negative lag in the UNC. A single significant zero-lag peak correlation was found between ATT_{perc} and RD_{perc} in the ILF, along with significant peak correlations at negative lag in the Fmajor, SLFT, and UNC (**Figure 5**).

Comparisons between AD_{perc} and RD_{perc} round significant zero-lag correlations in all tracts, while comparisons between FA_{perc} and both AD_{perc} and RD_{perc} found zero-lag correlations in the Fmajor, CCG, CST, SLFP, and UNC for both measures, along with significant correlations at negative lag in the SLFT. Comparisons between CBF_{perc} and ATT_{perc} found zero-lag correlations in the Fmajor, ILF, SLFT, and UNC.

DISCUSSION

We initially hypothesized that (1) tractwise microstructural and perfusion declines would not progress at the same rate in aging due to (2) earlier detectable declines in WM perfusion than microstructural integrity. Our findings support Hypothesis 1 and in part Hypothesis 2, but also highlight

the fact that the patterns of decline were much more varied both by tract and by measure than initially stated in Hypothesis 2.

MD was largely found to increase quadratically with age, while FA declined linearly in the majority of tracts. While this finding is in broad agreement with the aging literature (de Groot et al., 2016; Giorgio et al., 2010; Slater et al., 2019), FA was not uniformly associated with age across tracts, indicating variability in patterns or rates of WM decline. Across sexes, our microstructural results appear to indicate that fronto-inferior tracts decline at a relatively higher rate than those in the posterior WM (**Figure 3**). This appears consistent with existing anterior-posterior retrogenesis hypotheses (Hoagey et al., 2019; Slater et al., 2019), though the validity of this support remains to be tested. A notable exception to this is the CST, which will be discussed further in subsequent sections.

In addition to the well-established MD and FA associations with age, we also found significant and consistent CBF and ATT associations with age. Specifically, CBF declines with advancing age in the vast majority of WM tracts, mirroring the age-associated increases in tractwise MD (**Figure 2**). CBF appears to demonstrate a peak in middle-age, with the peak location varying by tract. Moreover, ATT demonstrates a robust linear increase with advancing age, consistent with previous reports (Mutsaerts et al., 2015).

Highest age effects on CBF appear to manifest in Fminor, CAB, ILF and SLFT, suggesting higher rates of vascular decline in the temporo-posterior WM than more anterior-superior tracts such as the Fmajor or CCG which demonstrate little to no CBF declines with age. This provides limited support for retrogenesis models predicting earlier or more rapid age declines in anterior regions (Brickman et al., 2012; Slater et al., 2019; Vik et al., 2015). However, patterns of age-related ATT increases across our tracts complicate this pattern. Despite showing some of the greeted CBF declines, Fmajor, CAB, and ILF tracts exhibited no significant ATT increases with age, making them notable outliers in our ATT analysis. This pattern suggests that ATT and CBF cannot be considered interchangeable measures of microvascular decline, and instead reflect different signatures or stages of microvascular aging that will require targeted analysis to clarify.

Understanding types of WM aging through multimodal integration

As revealed by the CCA, the interrelation between perfusion and microstructural integrity was similarly varied by tract. This highlights the importance of investigating the origins of this disparity. Moreover, rather than a smooth shared trajectory of decline, our evidence indicates the presence of different combinations of age effects: (i) significant and opposing loadings by CBF and AD; (ii) significant CBF contributions are accompanied by opposing RD contributions **(Figure 4**). In our belief, these signatures could be indicative of different probable types or even stages of WM aging:

(i) Marked mainly by effects on axial diffusivity, this could be an earlier stage of degeneration; the increasing AD accompanied by declining CBF is potentially due to the deterioration of crossing fibers resulting in RD increase of the secondary (perpendicular) fibre direction, which translates to AD increase in the principal fibre direction (Chad et al., 2018; Han et al., 2023). This anisotropic increase in diffusivity is consistent with an earlier stage of degeneration marked by declines in crossing association fibers prior to those in projection fibers (Han et al., 2023; Stadlbauer et al., 2008).

(ii) Marked by progressive demyelination of axon fibers, this could be a more advanced stage of degeneration; CBF decline is accompanied by increased RD, which, in the same crossing-fibre scenario, typically translates into myelin breakdown in the primary as well as secondary fiber bundles (Chad et al., 2021; Song et al., 2005), suggestive of a more advanced state of degeneration.

Interestingly, CST, a tract presumed to survive relatively robustly into later age (Michielse et al., 2010), falls into category (ii) in our CCA results. As the CST does exhibit the lowest MD increases and no significant differences in FA with age, there may be additional factors involved in maintaining this microstructural integrity despite perfusion declines. As axon diameter comparisons across the WM have observed relatively high mean diameter in CST fibers (Fan et al., 2020; Liewald et al., 2014), this may suggest fiber diameter in healthy WM as a predictor for resilience to perfusion declines.

As these two most common signatures of perfusion-microstructure association potentially represent different stages of an assumedly common sequence of decline (i.e. selective degeneration

followed by more uniform degeneration), the aforementioned mean axon diameter differences, or regional differences in number of vascular supplies, could also be associated with the degenerative signature observed. As myelination represents one of, if not the most significant factor in maintaining WM integrity with age (Hase et al., 2018; Kohama et al., 2012; Tang et al., 1997), differences in myelination trajectory and the ages at which regions fully myelinate may also play a part in determining regional robustness to perfusion changes. Additionally, our findings may reflect differing metabolic sensitivity to perfusion declines, as differing metabolic demands have been observed between larger and smaller fibers (Harris & Attwell, 2012). While WM is highly energy efficient in comparison to the cortex, the metabolic cost of maintaining myelin itself scales with fiber diameter. As a result, thicker fibers, such as those in the CST, require proportionally more resources to maintain in comparison to regions with relatively narrow fibers, such as the UNC. While thicker fibers appear more robust to microstructural declines, this could be offset by higher vascular demand. The interaction between higher microstructural resilience and higher vascular demand will require precise mapping of regional microvascular support to disentangle.

Furthermore, while FA draws considerable attention in aging research as a measure of microstructural integrity, our findings suggest that it contributes less to microstructural-perfusion interactions in aging than AD or RD. Even prior to examining tractwise variation across the brain, these results raise questions regarding established approaches that rely on FA for assessing WM microstructural declines with age. Our results indicate that other measures of microstructural decline are more sensitive to microstructural variations in the WM.

Sex differences in perfusion-microstructural variations in aging

Not only did perfusion-microstructure associations differ by tract, they also varied considerably between sexes (**Figure 6**). Overall, female subjects demonstrated a greater number of tracts with significant relationships between WM microstructure and perfusion, as well as proportionally more tracts

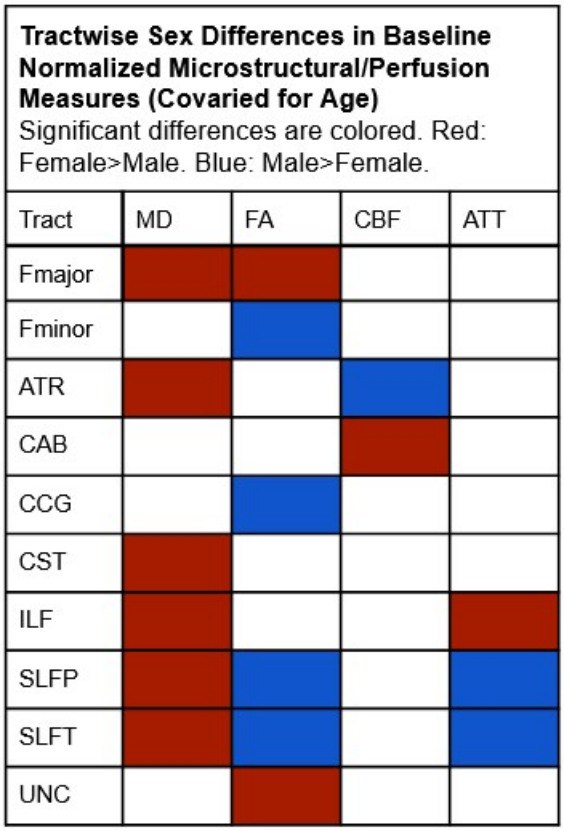

Figure 6: Tractwise sex differences in baseline normalized CBF, ATT, MD, and FA.

exhibiting signature (ii), suggesting a relatively more advanced state of decline in WM across the brain. This finding is consistent with previous reports (Intzandt et al., 2023; Patel et al., 2023). We speculate that a likely cause of these differences in WM aging by sex are the effects of menopause on brain health more broadly. Menopause has previously been found to affect structural, connectivity, and metabolic measures in the brain (Mosconi et al., 2021). Notably, cognitive impacts appear to stabilize post-menopause, though this is speculated to be the result of compensatory effects, rather than improvement in structural integrity. The sex differences with age observed in this study likely capture structural and microvascular impacts of peri- and postmenopause on the WM, though direct associations between these declines and cognitive performance will require additional investigation. Should microvascular declines be associated with cognitive performance similarly to the microstructural associations identified in this study, targeting vascular declines may benefit the study of interventions in the impacts of menopause on the brain in addition to the aging brain more generally. The degree to which hormone supplementation therapies may mitigate these effects, and indeed the mechanisms of estrogen's effects on WM health more generally, will require further investigation.

Temporal relationship in perfusion-microstructural variations in aging

The results of our cross-correlation analysis indicate that ATT may indeed precede microstructural declines in certain tracts. CBF, in contrast, appears to decline contemporaneously with microstructure. The superior sensitivity of vascular timing information to pathology is consistent with

recent reports on the unique sensitivity of vascular-response latency (Holmes et al., 2020; D. Kim et al., 2021; McKetton et al., 2019; Nanayakkara et al., 2023). In fact, ATT has previously been found to exhibit lower variability than CBF (Mutsaerts et al., 2015), which may underlie the finding that ATT, not CBF, displayed a detectable earlier variation in aging. Of the regions showing early rise in ATT, none but Fmajor exhibited a particularly high age effect in ATT or any of the other parameters investigated herein, arguing against a detectability bias due to age effect size (**Figure 3**). Moreover, implicated tracts (namely UNC, Fmajor and SLFP) do not show the same degenerative signatures as determined by their CCA results (**Figure 4**). Clarifying age lagged relationships in those tracts exhibiting linear declines will require either a wider age sample able to capture younger peak ATT values, or analysis of longitudinal data. Nonetheless, this is the first time that perfusion has been directly demonstrated as reflecting WM decline at an earlier age than does microstructure. Incorporating ATT, in addition to a more nuanced modeling of diffusion changes, may be necessary for similar investigations in future as we theorize that CBF and ATT reflect different, equally informative aspects of vascular aging.

Limitations

A notable limitation to these findings is that, while CBF declined quadratically in all tracts by the UNC, the predominantly linear declines in ATT restricted the extent of possible CCF comparisons. This raises the question of whether the age lagged effects found in the Fmajor, SLFT, and UNC can be taken as representative of WM declines more generally, or if this early detection on the part of ATT is unique to these tracts. As CBF declines in the Fminor lead microstructural declines despite contemporaneous declines between CBF and AD/RD in other tracts, the age at which these changes are detectable may also vary by tract. Additionally, CCF analysis depends on nonlinearity in the age-associations of its inputs. While many tracts demonstrated significant quadratic declines, the heterogeneity of significant quadratic versus linear age effects restricted the tracts in which cross-measure tractwise comparisons could be conducted. More generally, this study aimed to lay the groundwork for multimodal integration of aging metrics in the white matter and chose to address widely applied microstructural measures such as MD and

FA. This introduces a number of limitations that may be resolved in more advanced diffusion modeling. This study also addressed only ten major WM tracts. These were chosen to minimize tract overlap/partial-voluming between segmentations, however, additional comparisons may be possible in more recent segmentations (Maffei et al., 2021). Finally, while we have identified novel age-related findings using our paradigm, future exploration using longitudinal data would complement the cross-sectional nature of the HCP-A dataset used in this study.

Conclusions

Relationships between age, perfusion, and microstructural integrity assessed in this study depict highly tract-specific, as well as sex-specific, variation across our sample. The lack of a unified set of trends between perfusion and microstructural declines across tracts supports our hypothesis that WM perfusion and microstructure do not decline at the same rate in aging. Additionally, our secondary hypothesis that WM perfusion differences would be detectable earlier than differences in microstructural integrity, found limited support in evidence that tractwise age effect on ATT anticipate age effects in multiple microstructural measures. However, the ubiquity of CBF as a significant component in contemporaneous perfusion-microstructure relationships demonstrates that perfusion changes in the WM are complex and warrant greater attention in aging research. To our knowledge, this study is the first demonstration of tractwise declines in WM CBF and ATT with age, and these findings will be highly valuable to the development of a more unified model for mechanisms of brain aging.

Acknowledgments

We are grateful for the financial support from the Canadian Institutes of Health Research (CIHR) (#PTJ169688) and the Canada Research Chairs (CRC) program (JJC).

REFERENCES

Akashi, T., Takahashi, S., Mugikura, S., Sato, S., Murata, T., Umetsu, A., & Takase, K. (2017). Ischemic White Matter Lesions Associated With Medullary Arteries: Classification of MRI Findings Based on the Anatomic Arterial Distributions. *AJR. American Journal of Roentgenology*, *209*(3), W160–W168.

Baker, L. M., Laidlaw, D. H., Conturo, T. E., Hogan, J., Zhao, Y., Luo, X., Correia, S., Cabeen, R., Lane, E. M., Heaps, J. M., Bolzenius, J., Salminen, L. E., Akbudak, E., McMichael, A. R., Usher, C., Behrman, A., & Paul, R. H. (2014). White matter changes with age utilizing quantitative diffusion MRI. *Neurology*, *83*(3), 247–252.

Bender, A. R., Völkle, M. C., & Raz, N. (2016). Differential aging of cerebral white matter in middle-aged and older adults: A seven-year follow-up. *NeuroImage*, *125*, 74–83.

Bernbaum, M., Menon, B. K., Fick, G., Smith, E. E., Goyal, M., Frayne, R., & Coutts, S. B. (2015). Reduced blood flow in normal white matter predicts development of leukoaraiosis. *Journal of Cerebral Blood Flow and Metabolism: Official Journal of the International Society of Cerebral Blood Flow and Metabolism*, *35*(10), 1610–1615.

Bookheimer, S. Y., Salat, D. H., Terpstra, M., Ances, B. M., Barch, D. M., Buckner, R. L., Burgess, G. C., Curtiss, S. W., Diaz-Santos, M., Elam, J. S., Fischl, B., Greve, D. N., Hagy, H. A., Harms, M. P., Hatch, O. M., Hedden, T., Hodge, C., Japardi, K. C., Kuhn, T. P., … Yacoub, E. (2019). The Lifespan Human Connectome Project in Aging: An overview. *NeuroImage*, *185*, 335–348.

Brickman, A. M., Meier, I. B., Korgaonkar, M. S., Provenzano, F. A., Grieve, S. M., Siedlecki, K. L., Wasserman, B. T., Williams, L. M., & Zimmerman, M. E. (2012). Testing the white matter retrogenesis hypothesis of cognitive aging. *Neurobiology of Aging*, *33*(8), 1699–1715.

Chad, J. A., Pasternak, O., & Chen, J. J. (2021). Orthogonal moment diffusion tensor decomposition reveals age-related degeneration patterns in complex fiber architecture. *Neurobiology of Aging*, *101*, 150–159.

Chad, J. A., Pasternak, O., Salat, D. H., & Chen, J. J. (2018). Re-examining age-related differences in white matter microstructure with free-water corrected diffusion tensor imaging. *Neurobiology of Aging*, *71*, 161–170.

Chen, J. J., Rosas, H. D., & Salat, D. H. (2011). Age-associated reductions in cerebral blood flow are independent from regional atrophy. *NeuroImage*, *55*(2), 468–478.

Chen, J. J., Rosas, H. D., & Salat, D. H. (2013). The relationship between cortical blood flow and sub-cortical white-matter health across the adult age span. *PloS One*, *8*(2), e56733.

de Groot, M., Cremers, L. G. M., Ikram, M. A., Hofman, A., Krestin, G. P., van der Lugt, A., Niessen, W. J., & Vernooij, M. W. (2016). White Matter Degeneration with Aging: Longitudinal Diffusion MR Imaging Analysis. *Radiology*, *279*(2), 532–541.

de Groot, M., Ikram, M. A., Akoudad, S., Krestin, G. P., Hofman, A., van der Lugt, A., Niessen, W. J., & Vernooij, M. W. (2015). Tract-specific white matter degeneration in aging: the Rotterdam Study. *Alzheimer's & Dementia: The Journal of the Alzheimer's Association*, *11*(3), 321–330.

de la Torre, J. (2018). The Vascular Hypothesis of Alzheimer's Disease: A Key to Preclinical Prediction of Dementia Using Neuroimaging. *Journal of Alzheimer's Disease: JAD*, *63*(1), 35–52.

Fan, Q., Nummenmaa, A., Witzel, T., Ohringer, N., Tian, Q., Setsompop, K., Klawiter, E. C., Rosen, B. R., Wald, L. L., & Huang, S. Y. (2020). Axon diameter index estimation independent of fiber orientation distribution using high-gradient diffusion MRI. *NeuroImage*, *222*, 117197.

Giorgio, A., Santelli, L., Tomassini, V., Bosnell, R., Smith, S., De Stefano, N., & Johansen-Berg, H. (2010). Age-related changes in grey and white matter structure throughout adulthood. *NeuroImage*, *51*(3), 943–951.

Han, A., Dhollander, T., Sun, Y. L., Chad, J. A., & Chen, J. J. (2023). Fiber-specific age-related differences in the white matter of healthy adults uncovered by fixel-based analysis. *Neurobiology of Aging*, *130*, 22–29.

Harms, M. P., Somerville, L. H., Ances, B. M., Andersson, J., Barch, D. M., Bastiani, M., Bookheimer, S. Y., Brown, T. B., Buckner, R. L., Burgess, G. C., Coalson, T. S., Chappell, M. A., Dapretto, M.,

Douaud, G., Fischl, B., Glasser, M. F., Greve, D. N., Hodge, C., Jamison, K. W., … Yacoub, E. (2018). Extending the Human Connectome Project across ages: Imaging protocols for the Lifespan Development and Aging projects. *NeuroImage*, *183*, 972–984.

Harris, J. J., & Attwell, D. (2012). The energetics of CNS white matter. *The Journal of Neuroscience: The Official Journal of the Society for Neuroscience*, *32*(1), 356–371.

Hase, Y., Horsburgh, K., Ihara, M., & Kalaria, R. N. (2018). White matter degeneration in vascular and other ageing-related dementias. *Journal of Neurochemistry*, *144*(5), 617–633.

Hoagey, D. A., Rieck, J. R., Rodrigue, K. M., & Kennedy, K. M. (2019). Joint contributions of cortical morphometry and white matter microstructure in healthy brain aging: A partial least squares correlation analysis. *Human Brain Mapping*, *40*(18), 5315–5329.

Holmes, K. R., Tang-Wai, D., Sam, K., McKetton, L., Poublanc, J., Crawley, A. P., Sobczyk, O., Cohn, M., Duffin, J., Tartaglia, M. C., Black, S. E., Fisher, J. A., Wasserman, B., & Mikulis, D. J. (2020). Slowed Temporal and Parietal Cerebrovascular Response in Patients with Alzheimer's Disease. *The Canadian Journal of Neurological Sciences. Le Journal Canadien Des Sciences Neurologiques*, *47*(3), 366–373.

Intzandt, B., Sanami, S., Huck, J., PREVENT-AD Research group, Villeneuve, S., Bherer, L., & Gauthier, C. J. (2023). Sex-specific relationships between obesity, physical activity, and gray and white matter volume in cognitively unimpaired older adults. *GeroScience*. https://doi.org/10.1007/s11357-023-00734-4

Kim, C.-M., Alvarado, R. L., Stephens, K., Wey, H.-Y., Wang, D. J. J., Leritz, E. C., & Salat, D. H. (2020). Associations between cerebral blood flow and structural and functional brain imaging measures in individuals with neuropsychologically defined mild cognitive impairment. *Neurobiology of Aging*, *86*, 64–74.

Kim, D., Hughes, T. M., Lipford, M. E., Craft, S., Baker, L. D., Lockhart, S. N., Whitlow, C. T., Okonmah-Obazee, S. E., Hugenschmidt, C. E., Bobinski, M., & Jung, Y. (2021). Relationship Between Cerebrovascular Reactivity and Cognition Among People With Risk of Cognitive Decline.

Frontiers in Physiology, *12*, 645342.

Kobayashi, K., Hayashi, M., Nakano, H., Fukutani, Y., Sasaki, K., Shimazaki, M., & Koshino, Y. (2002). Apoptosis of astrocytes with enhanced lysosomal activity and oligodendrocytes in white matter lesions in Alzheimer's disease. *Neuropathology and Applied Neurobiology*, *28*(3), 238–251.

Kohama, S. G., Rosene, D. L., & Sherman, L. S. (2012). Age-related changes in human and non-human primate white matter: from myelination disturbances to cognitive decline. *Age* , *34*(5), 1093–1110.

Kohn, J. C., Lampi, M. C., & Reinhart-King, C. A. (2015). Age-related vascular stiffening: causes and consequences. *Frontiers in Genetics*, *6*, 112.

Lee, J. (2022). Near-Lifespan Tracking of Cerebral Microvascular Degeneration in Aging to Alzheimer's Continuum. *Advances in Geriatric Medicine and Research*, *4*(1). https://doi.org/10.20900/agmr20220003

Liewald, D., Miller, R., Logothetis, N., Wagner, H.-J., & Schüz, A. (2014). Distribution of axon diameters in cortical white matter: an electron-microscopic study on three human brains and a macaque. *Biological Cybernetics*, *108*(5), 541–557.

Li, Y., Choi, W. J., Wei, W., Song, S., Zhang, Q., Liu, J., & Wang, R. K. (2018). Aging-associated changes in cerebral vasculature and blood flow as determined by quantitative optical coherence tomography angiography. *Neurobiology of Aging*, *70*, 148–159.

Maffei, C., Lee, C., Planich, M., Ramprasad, M., Ravi, N., Trainor, D., Urban, Z., Kim, M., Jones, R. J., Henin, A., Hofmann, S. G., Pizzagalli, D. A., Auerbach, R. P., Gabrieli, J. D. E., Whitfield-Gabrieli, S., Greve, D. N., Haber, S. N., & Yendiki, A. (2021). Using diffusion MRI data acquired with ultra-high gradients to improve tractography in routine-quality data. In *bioRxiv* (p. 2021.06.28.450265). https://doi.org/10.1101/2021.06.28.450265

Mayer, C., Frey, B. M., Schlemm, E., Petersen, M., Engelke, K., Hanning, U., Jagodzinski, A., Borof, K., Fiehler, J., Gerloff, C., Thomalla, G., & Cheng, B. (2021). Linking cortical atrophy to white matter hyperintensities of presumed vascular origin. *Journal of Cerebral Blood Flow and Metabolism: Official Journal of the International Society of Cerebral Blood Flow and Metabolism*, *41*(7), 1682–

1691.

McKetton, L., Cohn, M., Tang-Wai, D. F., Sobczyk, O., Duffin, J., Holmes, K. R., Poublanc, J., Sam, K., Crawley, A. P., Venkatraghavan, L., Fisher, J. A., & Mikulis, D. J. (2019). Cerebrovascular Resistance in Healthy Aging and Mild Cognitive Impairment. *Frontiers in Aging Neuroscience*, *11*, 79.

Michielse, S., Coupland, N., Camicioli, R., Carter, R., Seres, P., Sabino, J., & Malykhin, N. (2010). Selective effects of aging on brain white matter microstructure: a diffusion tensor imaging tractography study. *NeuroImage*, *52*(4), 1190–1201.

Mosconi, L., Berti, V., Dyke, J., Schelbaum, E., Jett, S., Loughlin, L., Jang, G., Rahman, A., Hristov, H., Pahlajani, S., Andrews, R., Matthews, D., Etingin, O., Ganzer, C., de Leon, M., Isaacson, R., & Brinton, R. D. (2021). Menopause impacts human brain structure, connectivity, energy metabolism, and amyloid-beta deposition. *Scientific Reports*, *11*(1), 10867.

Mutsaerts, H. J. M. M., van Dalen, J. W., Heijtel, D. F. R., Groot, P. F. C., Majoie, C. B. L. M., Petersen, E. T., Richard, E., & Nederveen, A. J. (2015). Cerebral Perfusion Measurements in Elderly with Hypertension Using Arterial Spin Labeling. *PloS One*, *10*(8), e0133717.

Nanayakkara, N. D., Meusel, L.-A., Anderson, N. D., & Chen, J. J. (2023). Robust estimation of dynamic cerebrovascular reactivity using breath-holding fMRI: application in diabetes and hypertension. In *medRxiv*. https://doi.org/10.1101/2023.05.20.23290209

Nonaka, H., Akima, M., Hatori, T., Nagayama, T., Zhang, Z., & Ihara, F. (2003). Microvasculature of the human cerebral white matter: arteries of the deep white matter. *Neuropathology: Official Journal of the Japanese Society of Neuropathology*, *23*(2), 111–118.

Nozais, V., Forkel, S. J., Foulon, C., Petit, L., & Thiebaut de Schotten, M. (2021). Functionnectome as a framework to analyse the contribution of brain circuits to fMRI. *Communications Biology*, *4*(1), 1035.

O'Sullivan, M., Lythgoe, D. J., Pereira, A. C., Summers, P. E., Jarosz, J. M., Williams, S. C. R., & Markus, H. S. (2002). Patterns of cerebral blood flow reduction in patients with ischemic

leukoaraiosis. *Neurology*, *59*(3), 321–326.

Patel, A., Chad, J. A., & Chen, J. J. (2023). Is adiposity associated with white matter microstructural health and intelligence differently in males and females? *Obesity* , *31*(4), 1011–1023.

Robinson, T. D., Sun, Y. L., Chang, P. T. H., & Jean Chen, J. (2023). In search of a unifying theory of white matter aging: tract morphometry-microstructure relationships. In *bioRxiv* (p. 2023.03.14.532658). https://doi.org/10.1101/2023.03.14.532658

Sala, S., Agosta, F., Pagani, E., Copetti, M., Comi, G., & Filippi, M. (2012). Microstructural changes and atrophy in brain white matter tracts with aging. *Neurobiology of Aging*, *33*(3), 488–498.e2.

Schilling, K. G., Archer, D., Yeh, F.-C., Rheault, F., Cai, L. Y., Hansen, C., Yang, Q., Ramdass, K., Shafer, A. T., Resnick, S. M., Pechman, K. R., Gifford, K. A., Hohman, T. J., Jefferson, A., Anderson, A. W., Kang, H., & Landman, B. A. (2022). Aging and white matter microstructure and macrostructure: a longitudinal multi-site diffusion MRI study of 1218 participants. *Brain Structure & Function*, *227*(6), 2111–2125.

Slater, D. A., Melie-Garcia, L., Preisig, M., Kherif, F., Lutti, A., & Draganski, B. (2019). Evolution of white matter tract microstructure across the life span. *Human Brain Mapping*, *40*(7), 2252–2268.

Smirnov, M., Destrieux, C., & Maldonado, I. L. (2021). Cerebral white matter vasculature: still uncharted? *Brain: A Journal of Neurology*, *144*(12), 3561–3575.

Song, S.-K., Yoshino, J., Le, T. Q., Lin, S.-J., Sun, S.-W., Cross, A. H., & Armstrong, R. C. (2005). Demyelination increases radial diffusivity in corpus callosum of mouse brain. *NeuroImage*, *26*(1), 132–140.

Stadlbauer, A., Salomonowitz, E., Strunk, G., Hammen, T., & Ganslandt, O. (2008). Age-related degradation in the central nervous system: assessment with diffusion-tensor imaging and quantitative fiber tracking. *Radiology*, *247*(1), 179–188.

Stricker, N. H., Schweinsburg, B. C., Delano-Wood, L., Wierenga, C. E., Bangen, K. J., Haaland, K. Y., Frank, L. R., Salmon, D. P., & Bondi, M. W. (2009). Decreased white matter integrity in late-myelinating fiber pathways in Alzheimer's disease supports retrogenesis. *NeuroImage*, *45*(1), 10–16.

Tang, Y., Nyengaard, J. R., Pakkenberg, B., & Gundersen, H. J. (1997). Age-induced white matter changes in the human brain: a stereological investigation. *Neurobiology of Aging*, *18*(6), 609–615.

Tomoto, T., Tarumi, T., & Zhang, R. (2023). Central arterial stiffness, brain white matter hyperintensity and total brain volume across the adult lifespan. *Journal of Hypertension*, *41*(5), 819–829.

Vik, A., Hodneland, E., Haász, J., Ystad, M., Lundervold, A. J., & Lundervold, A. (2015). Fractional anisotropy shows differential reduction in frontal-subcortical fiber bundles—A longitudinal MRI study of 76 middle-aged and older adults. *Frontiers in Aging Neuroscience*, *7*. https://doi.org/10.3389/fnagi.2015.00081

Wierenga, C. E., Hays, C. C., & Zlatar, Z. Z. (2014). Cerebral blood flow measured by arterial spin labeling MRI as a preclinical marker of Alzheimer's disease. *Journal of Alzheimer's Disease: JAD*, *42 Suppl 4*(Suppl 4), S411–S419.

Yeatman, J. D., Wandell, B. A., & Mezer, A. A. (2014). Lifespan maturation and degeneration of human brain white matter. *Nature Communications*, *5*, 4932.

Yendiki, A., Panneck, P., Srinivasan, P., Stevens, A., Zöllei, L., Augustinack, J., Wang, R., Salat, D., Ehrlich, S., Behrens, T., Jbabdi, S., Gollub, R., & Fischl, B. (2011). Automated probabilistic reconstruction of white-matter pathways in health and disease using an atlas of the underlying anatomy. *Frontiers in Neuroinformatics*, *5*, 23.

Zhang, N., Gordon, M. L., Ma, Y., Chi, B., Gomar, J. J., Peng, S., Kingsley, P. B., Eidelberg, D., & Goldberg, T. E. (2018). The Age-Related Perfusion Pattern Measured With Arterial Spin Labeling MRI in Healthy Subjects. *Frontiers in Aging Neuroscience*, *10*, 214.

Zlokovic, B. V. (2011). Neurovascular pathways to neurodegeneration in Alzheimer's disease and other disorders. *Nature Reviews. Neuroscience*, *12*(12), 723–738.

Supplementary Materials

Supplementary Table 1a: Model 1 - Whole-WM MD/FA Relationships with Perfusion (Covaried for Sex).
All models are multivariate linear regressions based on baseline-normalized measures (x_{perc}) with overall F-statistics, *p*-values, and effect sizes ($R^2_{adjusted}$) listed. Slopes are noted below each regression equation and significant associations bolded with asterisks indicating significance. (*:p<.05, **:p<.01, ***:p<.001).

	MD_{perc}		**FA_{perc}**	
Tract	CBF_{perc}	ATT_{perc}	CBF_{perc}	ATT_{perc}
All	$F(2, 497) = 5.36$, $p = .005$, $R^2_{Adjusted} = .02$	$F(2, 497) = 4.07$, $p = .02$, $R^2_{Adjusted} = .01$	$F(2, 497) = 0.40$, $p = .67$, $R^2_{Adjusted} = -.002$	$F(2, 497) = 0.02$, $p = .98$, $R^2_{Adjusted} = -.004$
	-0.018508**	**0.231872***	0.0089404	0.0060844

Supplementary Table 1b: Model 1 - Tractwise MD/FA Relationships with Perfusion (Covaried for Sex).
All models are multivariate linear regressions based on baseline-normalized measures (x_{perc}) with overall F-statistics, *p*-values, and effect sizes ($R^2_{adjusted}$) listed. Slopes are noted below each regression equation and significant associations bolded with asterisks indicating significance. (*:p<.05, **:p<.01, ***:p<.001).

	MD_{perc}		**FA_{perc}**	
Tract	CBF_{perc}	ATT_{perc}	CBF_{perc}	ATT_{perc}
Fmajor	$F(2, 490) = 7.47$, $p < .001$, $R^2_{Adjusted} = .03$	$F(2, 490) = 5.68$, $p = .004$, $R^2_{Adjusted} = .02$	$F(2, 490) = 8.24$, $p < .001$, $R^2_{Adjusted} = .03$	$F(2, 490) = 8.08$, $p < .001$, $R^2_{Adjusted} = .03$
	-0.009599	0.081493	-0.003605	-0.010087
Fminor	$F(2, 490) = 1.52$, $p = .22$, $R^2_{Adjusted} = .002$	$F(2, 490) = 6{,}48$, $p = .002$, $R^2_{Adjusted} = .02$	$F(2, 490) = 5.49$, $p = .004$, $R^2_{Adjusted} = .02$	$F(2, 490) = 5.53$, $p = .004$, $R^2_{Adjusted} = .02$

	-0.011735	**0.289540****	0.019804	-0.227797
ATR	$F(2, 494) = 2.08$, $p = .13$, $R^2_{Adjusted} = .004$	$F(2, 494) = 9.13$, $p < .001$, $R^2_{Adjusted} = .03$	$F(2, 494) = 3.23$, $p = .009$, $R^2_{Adjusted} = .04$	$F(2, 494) = 4.22$, $p = .015$, $R^2_{Adjusted} = .01$
	-0.014611	**0.324941*****	0.027963	**-0.306558****
CAB	$F(2, 487) = 0.47$, $p = .62$, $R^2_{Adjusted} = -.002$	$F(2, 487) = 2.69$, $p = .07$, $R^2_{Adjusted} = .007$	$F(2, 487) = 0.75$, $p = .47$, $R^2_{Adjusted} = -.001$	$F(2, 487) = 4.53$, $p = .01$, $R^2_{Adjusted} = .01$
	0.0006211	-0.202510	0.01026	**0.79903***
CCG	$F(2, 492) = 2.48$, $p = .085$, $R^2_{Adjusted} = .006$	$F(2, 492) = 4.82$, $p = .008$, $R^2_{Adjusted} = .02$	$F(2, 492) = 13.3$, $p < .001$, $R^2_{Adjusted} = .05$	$F(2, 492) = 2.60$, $p = .006$, $R^2_{Adjusted} = .08$
	-0.013649	**0.216401****	**0.068524*****	0.050215
CST	$F(2, 488) = 6.42$, $p = .002$, $R^2_{Adjusted} = .02$	$F(2, 488) = 6.19$, $p = .002$, $R^2_{Adjusted} = .02$	$F(2, 488) = 1.89$, $p = .15$, $R^2_{Adjusted} = .004$	$F(2, 488) = 1.80$, $p = .17$, $R^2_{Adjusted} = .003$
	-0.006782	0.050971	-0.018407	0.225689
ILF	$F(2, 494) = 8.03$, $p < .001$, $R^2_{Adjusted} = .03$	$F(2, 494) = 3.67$, $p = .026$, $R^2_{Adjusted} = .01$	$F(2, 494) = 2.28$, $p = .10$, $R^2_{Adjusted} = .005$	$F(2, 494) = 2.90$, $p = .06$, $R^2_{Adjusted} = .008$
	-0.019481*	-0.032828	0.004481	0.16351
SLFP	$F(2, 494) = 3.64$, $p = .027$, $R^2_{Adjusted} = .01$	$F(2, 494) = 5.51$, $p = .004$, $R^2_{Adjusted} = .02$	$F(2, 494) = 2.15$, $p = .12$, $R^2_{Adjusted} = .005$	$F(2, 494) = 4.46$, $p = .012$, $R^2_{Adjusted} = .01$
	-0.014721	**0.214620***	-0.007393	-0.247955

SLFT	$F(2, 492) = 5.01$, $p = .007$, $R^2_{Adjusted} = .02$	$F(2, 492) = 7.78$, $p = .008$, $R^2_{Adjusted} = .02$	$F(2, 492) = 4.99$, $p = .007$, $R^2_{Adjusted} = .02$	$F(2, 492) = 3.37$, $p = .035$, $R^2_{Adjusted} = .009$
	-0.021370*	**0.222030***	-0.021391	-0.127256
UNC	$F(2, 492) = 0.49$, $p = .61$, $R^2_{Adjusted} = -.002$	$F(2, 492) = 0.82$, $p = .44$, $R^2_{Adjusted} = -.0007$	$F(2, 492) = 5.06$, $p = .007$, $R^2_{Adjusted} = .02$	$F(2, 492) = 4.33$, $p = .014$, $R^2_{Adjusted} = .01$
	-0.0055602	0.1058895	0.015398	-0.143507

Supplementary Table 2a: Model 2 - Whole-WM Sex Differences in Relationships Between MD/FA and Perfusion (Covaried for Age).
All models are multivariate linear regressions based on baseline-normalized measures (x_{perc}) with overall F-statistics, *p*-values, and effect sizes ($R^2_{adjusted}$) listed. Slopes are noted below each regression equation and significant associations bolded with asterisks indicating significance. (*:p<.05, **:p<.01, ***:p<.001).

	MD_{perc}				**FA_{perc}**			
	CBF_{perc}		ATT_{perc}		CBF		ATT	
Tract	Female	Male	Female	Male	Female	Male	Female	Male
All	$F(2, 291) = 55.5$, $p < .001$, $R^2_{Adjusted} = .27$	$F(2, 203) = 33.2$, $p < .001$, $R^2_{Adjusted} = .17$	$F(2, 291) = 55.1$, $p < .001$, $R^2_{Adjusted} = .27$	$F(2, 203) = 22.3$, $p < .001$, $R^2_{Adjusted} = .17$	$F(2, 291) = 9.72$, $p < .001$, $R^2_{Adjusted} = .06$	$F(2, 203) = 1.86$, $p = .16$, $R^2_{Adjusted} = .008$	$F(2, 291) = 9.51$, $p < .001$, $R^2_{Adjusted} = .05$	$F(2, 203) = 1.60$, $p = .20$, $R^2_{Adjusted} = .006$
	-0.0079527	-0.0007841	0.0559703	-0.0668848	0.0130418	-0.0143295	0.1261818	0.1857851

Supplementary Table 2b: Model 2 - Tractwise Sex Differences in Relationships Between MD/FA and Perfusion (Covaried for Age).
All models are multivariate linear regressions based on baseline-normalized measures (x_{perc}) with overall F-statistics, *p*-values, and effect sizes ($R^2_{adjusted}$) listed. Slopes are noted below each regression equation and significant associations bolded with asterisks indicating significance. (*:p<.05, **:p<.01, ***:p<.001).

	MD_{perc}				**FA_{perc}**			
	CBF_{perc}		ATT_{perc}		CBF_{perc}		$ATT_{percentage}$	
Tract	Female	Male	Female	Male	Female	Male	Female	Male
Fmajor	$F(2, 287) = 31.3$, $p < .001$, $R^2_{Adjusted} = .17$	$F(2, 200) = 9.30$, $p < .001$, $R^2_{Adjusted} = .009$	$F(2, 287) = 32.9$, $p < .001$, $R^2_{Adjusted} = .18$	$F(2, 200) = 8.95$, $p < .001$, $R^2_{Adjusted} = .07$	$F(2, 287) = 3.44$, $p = .034$, $R^2_{Adjusted} = .02$	$F(2, 200) = 1.96$, $p = .14$, $R^2_{Adjusted} = .009$	$F(2, 287) = 2.92$, $p = .056$, $R^2_{Adjusted} = .01$	$F(2, 200) = 1.96$, $p = .14$, $R^2_{Adjusted} = .009$
	-0.0039667	-0.0076777	0.1285074	0.0116263	-0.0093200	-0.0026277	-0.0444465	0.0518249
Fminor	$F(2, 288) = 77.5$, $p < .001$, $R^2_{Adjusted} = .35$	$F(2, 199) = 26.6$, $p < .001$, $R^2_{Adjusted} = .20$	$F(2, 288) = 76.8$, $p < .001$, $R^2_{Adjusted} = .34$	$F(2, 199) = 26.7$, $p < .001$, $R^2_{Adjusted} = .20$	$F(2, 288) = 24.4$, $p < .001$, $R^2_{Adjusted} = .14$	$F(2, 199) = 10.6$, $p < .001$, $R^2_{Adjusted} = .09$	$F(2, 288) = 22.0$, $p < .001$, $R^2_{Adjusted} = .13$	$F(2, 199) = 10.6$, $p < .001$, $R^2_{Adjusted} = .09$
	-0.0093523	-0.0011248	0.0490044	0.0443195	0.0248039	0.0045800	-0.0178029	-0.061765
ATR	$F(2, 289) = 63.6$, $p < .001$, $R^2_{Adjusted} = .30$	$F(2, 202) = 32.7$, $p < .001$, $R^2_{Adjusted} = .24$	$F(2, 289) = 65.0$, $p < .001$, $R^2_{Adjusted} = .31$	$F(2, 202) = 32.3$, $p < .001$, $R^2_{Adjusted} = .23$	$F(2, 289) = 8.25$, $p < .001$, $R^2_{Adjusted} = .05$	$F(2, 202) = 0.25$, $p = .78$, $R^2_{Adjusted} = -.007$	$F(2, 289) = 8.44$, $p < .001$, $R^2_{Adjusted} = .05$	$F(2, 202) = 0.08$, $p = .92$, $R^2_{Adjusted} = -.009$
	-0.0023397	-0.0075814	0.1296512	-0.0436909	**0.0427019***	0.0094317	**-0.3579011***	-0.0112258
CAB	$F(2, 285) = 14.5$, $p < .001$, $R^2_{Adjusted} = .09$	$F(2, 199) = 2.56$, $p = .08$, $R^2_{Adjusted} = .02$	$F(2, 285) = 14.3$, $p < .001$, $R^2_{Adjusted} = .08$	$F(2, 199) = 4.17$, $p = .016$, $R^2_{Adjusted} = .03$	$F(2, 285) = 7.74$, $p < .001$, $R^2_{Adjusted} = .04$	$F(2, 199) = 4.04$, $p = .02$, $R^2_{Adjusted} = .03$	$F(2, 285) = 11.2$, $p < .001$, $R^2_{Adjusted} = .07$	$F(2, 199) = 4.68$, $p = .01$, $R^2_{Adjusted} = .04$

	0.0114287	0.0064030	-0.1455464	-0.3302063	-0.0086050	-0.0161303	**0.7990257***	0.7374741
CCG	$F(2, 289) = 41.1$, $p < .001$, $R^2_{Adjusted} = .22$	$F(2, 200) = 18.6$, $p < .001$, $R^2_{Adjusted} = .15$	$F(2, 289) = 42.5$, $p < .001$, $R^2_{Adjusted} = .22$	$F(2, 200) = 18.4$, $p < .001$, $R^2_{Adjusted} = .15$	$F(2, 289) = 17.9$, $p < .001$, $R^2_{Adjusted} = .10$	$F(2, 200) = 11.5$, $p < .001$, $R^2_{Adjusted} = .09$	$F(2, 289) = 14.8$, $p < .001$, $R^2_{Adjusted} = .09$	$F(2, 200) = 6.26$, $p = .002$, $R^2_{Adjusted} = .05$
	-0.010615	-0.0046832	0.1605160	-0.0354249	**0.0482986***	**0.0755159*****	0.107982	0.5138831
CST	$F(2, 284) = 9.29$, $p < .001$, $R^2_{Adjusted} = .05$	$F(2, 201) = 1.37$, $p = .26$, $R^2_{Adjusted} = .004$	$F(2, 284) = 9.60$, $p < .001$, $R^2_{Adjusted} = .06$	$F(2, 201) = 1.35$, $p = .26$, $R^2_{Adjusted} = .003$	$F(2, 284) = 0.97$, $p = .38$, $R^2_{Adjusted} = -.0002$	$F(2, 201) = 3.67$, $p = .03$, $R^2_{Adjusted} = .03$	$F(2, 284) = 1.97$, $p = .14$, $R^2_{Adjusted} = .007$	$F(2, 201) = 1.29$, $p = .28$, $R^2_{Adjusted} = .003$
	0.0061903	-0.0065296	-0.1043070	0.0842141	-0.0054017	**-0.03705****	0.2295747	0.3193
ILF	$F(2, 289) = 43.0$, $p < .001$, $R^2_{Adjusted} = .22$	$F(2, 202) = 17.7$, $p < .001$, $R^2_{Adjusted} = .14$	$F(2, 289) = 41.8$, $p < .001$, $R^2_{Adjusted} = .22$	$F(2, 202) = 17.7$, $p < .001$, $R^2_{Adjusted} = .14$	$F(2, 289) = 10.3$, $p < .001$, $R^2_{Adjusted} = .06$	$F(2, 202) = 3.82$, $p = .02$, $R^2_{Adjusted} = .03$	$F(2, 289) = 10.7$, $p < .001$, $R^2_{Adjusted} = .06$	$F(2, 202) = 3.50$, $p = .03$, $R^2_{Adjusted} = .02$
	-0.0125893	0.0018092	0.0240348	0.0051664	-0.0020199	-0.0112217	0.1423583	0.0884416
SLFP	$F(2, 288) = 47.8$, $p < .001$, $R^2_{Adjusted} = .24$	$F(2, 203) = 20.6$, $p < .001$, $R^2_{Adjusted} = .16$	$F(2, 288) = 48.1$, $p < .001$, $R^2_{Adjusted} = .25$	$F(2, 203) = 20.8$, $p < .001$, $R^2_{Adjusted} = .16$	$F(2, 288) = 7.54$, $p < .001$, $R^2_{Adjusted} = .04$	$F(2, 203) = 1.73$, $p = .18$, $R^2_{Adjusted} = .007$	$F(2, 288) = 8,76$, $p < .001$, $R^2_{Adjusted} = .05$	$F(2, 203) = 0.41$, $p = .67$, $R^2_{Adjusted} = -.006$
	-0.0059281	0.0023829	0.0836243	0.0632643	-0.00005828	-0.02840	-0.2094319	-0.1595419
SLFT	$F(2, 287) = 52.9$, $p < .001$, $R^2_{Adjusted} = .26$	$F(2, 202) = 22.2$, $p < .001$, $R^2_{Adjusted} = .17$	$F(2, 287) = 53.6$, $p < .001$, $R^2_{Adjusted} = .27$	$F(2, 202) = 22.3$, $p < .001$, $R^2_{Adjusted} = .17$	$F(2, 287) = 4.30$, $p = .014$, $R^2_{Adjusted} = .02$	$F(2, 202) = 6.02$, $p = .003$, $R^2_{Adjusted} = .05$	$F(2, 287) = 4.59$, $p = .011$, $R^2_{Adjusted} = .02$	$F(2, 202) = 1.80$, $p = .17$, $R^2_{Adjusted} = .008$
	-0.0078787	0.0006048	0.1188965	0.0478854	-0.0097048	**-0.0440165****	-0.1308776	-0.0510914

UNC	$F(2, 290) = 49.5$, $p < .001$, $R^2_{Adjusted} = .25$	$F(2, 199) = 18.4$, $p < .001$, $R^2_{Adjusted} = .15$	$F(2, 290) = 49.8$ $p < .001$, $R^2_{Adjusted} = .25$	$F(2, 199) = 18.4$, $p < .001$, $R^2_{Adjusted} = .15$	$F(2, 290) = 3.21$, $p = .04$, $R^2_{Adjusted} = .01$	$F(2, 199) = 0.30$, $p = .74$, $R^2_{Adjusted} = -.007$	$F(2, 290) = 1.28$, $p = .28$, $R^2_{Adjusted} = .002$	$F(2, 199) = 0.32$, $p = .73$, $R^2_{Adjusted} = -.007$
	0.00004331	0.0009167	0.0632672	-0.0315701	0.0289662	-0.0053114	-0.1422849	-0.0935715